Modular networks with delayed coupling: Synchronization and frequency control

Oleg V. Maslennikov* and Vladimir I. Nekorkin
Institute of Applied Physics of RAS, Nizhny Novgorod, Russia
and N. I. Lobachevsky State University of Nizhny Nodgorod, Nizhny Novgorod, Russia
(Received 11 March 2014; published 3 July 2014)

We study the collective dynamics of modular networks consisting of map-based neurons which generate irregular spike sequences. Three types of intramodule topology are considered: a random Erdös-Rényi network, a small-world Watts-Strogatz network, and a scale-free Barabási-Albert network. The interaction between the neurons of different modules is organized by relatively sparse connections with time delay. For all the types of the network topology considered, we found that with increasing delay two regimes of module synchronization alternate with each other: inphase and antiphase. At the same time, the average rate of collective oscillations decreases within each of the time-delay intervals corresponding to a particular synchronization regime. A dual role of the time delay is thus established: controlling a synchronization mode and degree and controlling an average network frequency. Furthermore, we investigate the influence on the modular synchronization by other parameters: the strength of intermodule coupling and the individual firing rate.

DOI: 10.1103/PhysRevE.90.012901 PACS number(s): 05.45.Xt, 89.75.Fb

I. INTRODUCTION

The formation of spatiotemporal patterns of electrical activity, their synchronization, and desynchronization is one of the main phenomena observed in cortical brain structures during normal cognitive functioning as well as different pathologies [1,2]. Based on experimental data, one can usually distinguish several spatially isolated regions that display coordinated activity, in the simplest case, in the form of inphase and antiphase clusters. Each of those clusters comprises a group of neurons generating highly synchronous spikes during certain time intervals. A global network connectivity underlying such behavior may be presented as a set of modules (subnetworks, populations) which consist of densely coupled neurons and interact with each other by relatively sparse connections [3–6]. Despite a significant progress in understanding a large-scale cortico-cortical connectome, detailed information is still lacking about coupling features at the neuronal level. Thus, uncovering properties of the intramodule structure, individual neuron dynamics and intermodule coupling is a topical problem since these features have a great impact on the coordinated behavior of different regions. Among a variety of factors, one can highlight delayed coupling between different modules so the joint effect of the modularity and intermodule delayed coupling on the network dynamics is a problem of great interest. It should be noted that most of the research in this direction has mainly taken into account the indicated factors separately. The studies that can be carried to the first group are devoted to how the delayed coupling influences the network dynamics without regard to modularity. The papers of the second group consider the role of modularity in different network activity regimes, but do not take into account delayed intermodule coupling. In addition, there are some studies on modular networks with delayed coupling, however, there are still many problems to be solved.

The first group consists of the studies which analyze the effect of time-delayed connections in networks. Note that the phenomenon of synchronization arising in networks of active elements due to delayed interelement interaction has recently attracted much attention, see, e.g., the surveys in Refs. [7,8]. The analysis of networks of various nature has revealed that the collective dynamics significantly depends on the value of delay. It was found for a scale-free network [9] of map-based neurons [10] interacting by electrical synapses that, with increasing delay synchronous and asynchronous modes alternate with each other appearing at multiples of the oscillation frequency. Larger coupling strength results in that the intervals of time delay corresponding to the synchronous regime as well as the synchronization degree increase. The same effect of alternation between synchronous and asynchronous regimes with increasing time delay was observed in networks with different topologies (in particular, small-world networks) and different interaction types (electrical and chemical synapses) [11–17]. The influence of the other factors such as the coupling strength, the fraction of electrical synapses, and a denser network structure does not significantly change the effect of alternation although it increases the synchronization degree and broadens the intervals of time delay corresponding to the synchronous regime. It should be noted that the interaction delay may affect not only a regime of synchronization but also other features of collective network dynamics. For example, the authors of Ref. [18] showed that in random networks of bursting neurons the time delay influences the synchronization degree and the average frequency of burst network oscillations, at the same time an enhancement of the phase synchronization is accompanied by increasing the average burst frequency.

The second group consists of studies which take into account the modularity, i.e., the presence of distinguished groups of neurons which can have a considerable impact on the collective dynamics, in particular, clusters of synchronous activity can appear [19]. What type of behavior (synchronous or asynchronous) is observed in this case significantly depends on the parameters of intermodule and intramodule coupling. In Ref. [20] a network of several small-world modules was considered which consists of map-based neurons displaying burst oscillations at the individual level. It was shown that

*olmaov@neuron.appl.sci-nnov.ru

the phase synchronization in such a modular network appears for a high-enough probability of intermodule coupling and for the coupling strength larger than some critical value which was found by the reduction to a network of phase oscillators. In Ref. [21] an opposite problem was solved: how to suppress burst synchronization in a modular network. The authors showed that if the modules have scale-free topology, an effective method of suppression is the deactivation of a specially selected neuron.

One can naturally expect that the time delay in modular networks leads to new effects of collective dynamics and synchronization. The dynamics of modular networks was considered in Refs. [22,23] with time delays which were taken the same for the intramodule and intermodule connections. Increasing the time delay results in the phenomenon of alternation between synchronous and asynchronous regimes described above. However, in real networks the interaction between neurons belonging to different regions can occur with a larger time delay compared to that within the modules, and this can lead to a variety of new regimes of collective dynamics. Interesting results in this direction are presented in a series of papers [24–27] where the authors studied the role of intermodule delay in cluster synchronization. One of the striking conclusions is about a nonlocal mechanism which underlies cluster formation and is based on the greatest common divisor (GCD) of circuit delay loops. For example, if a neural network is a set of modules interacting with delay and connected into several closed loops then the maximum number of clusters of synchronized neurons is equal to the GCD of these loops when some module is stimulated. If the network is simulated by a complex stimulus, i.e., when several modules receive input signals the number of clusters can be any common divisor of delay loops. The theoretical results were supported by experimental *in vitro* investigations [28,29].

In this paper, we consider a modular network where intramodule coupling is instantaneous while the elements of different modules interact with time delay. Such a model reflects the property of cortical networks that are spatially remote from each other and thus they interact with time delay. As a module, we use complex networks with three different topologies (see, e.g., Ref. [30]): a random Erdös-Rényi network, a small-world Watts-Strogatz network, and a scale-free Barabási-Albert network; each of them more or less reproduces the structure properties of real neural networks. The interaction between the modules is performed by relatively sparse connections with time delay. Individual neural dynamics in our model are described by the discrete-time model [31,32] which mimics irregular spiking sequences. For the intramodule topologies indicated we show that with increasing time delay, the inphase and antiphase regimes of modular synchronization alternate with each other. Moreover, with increasing time delay the network oscillations change their frequency, namely, within every delay interval corresponding to a certain synchronization regime the frequency decreases on the average. Also we study how the collective activity is influenced by the intermodule coupling strength and the average spike rate of individual neurons.

The paper is organized as follows. In Sec. II we briefly describe the algorithms for creating a modular network and discuss the main properties of individual dynamics displayed by map-based neurons. Then, in Sec. III we consider regimes of synchronous activity depending on intermodule delayed coupling as well as other parameters. Finally, in Sec. IV we draw conclusions and discuss the main results.

II. MODEL

A. Network structure

Consider a network which is constituted by two interacting subnetworks-modules schematically shown in Fig. 1. Each module consists of N active nodes coupled with each other by directed links which model the chemical synapses. Following the experimental observations [33], we set 80% of the total number of neurons sending excitatory connections while the remaining 20% of the neurons were set as inhibitory. We consider three different algorithms for generating an intramodule connection topology: a random Erdös-Rényi network, a small-world Watts-Strogatz network, and a scale-free Barabási-Albert network, in every case with directed links. The connections between the modules are random and relatively sparse: 5% of nodes in one module send directed excitatory links to random nodes of another module (note that the nodes are chosen from those 80% which send excitatory connections inside their module to which they belong). In the following we are mainly interested in the impact of the strength of intermodule coupling g_o and its time delay τ.

The three topologies indicated are well known in the network science and with good accuracy describe the structure of local connections in neural circuits. Note that in all cases we use *directed* network modifications because we consider chemical interactions between neurons. The directed network is characterized by the parameter p_{dir}, a probability of a mutual (bidirectional) connection to appear between a pair of nodes. The main difference between the algorithms of building directed and undirected networks is the following. Suppose, according to a certain rule of network creation it is necessary to attach the jth node to the ith node. With probability p_{dir} a bidirectional link is created between them, in the opposite

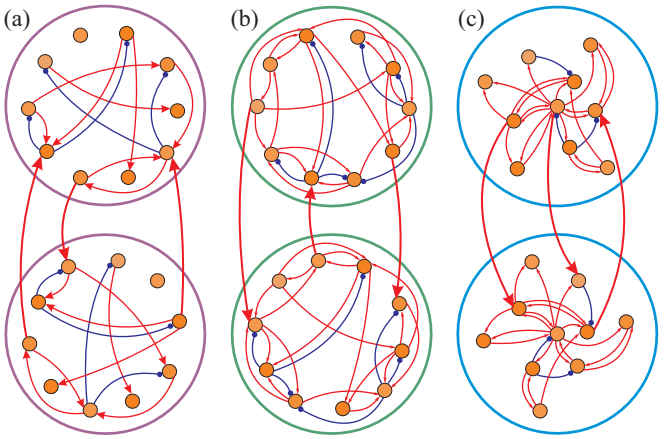

FIG. 1. (Color online) Structure of a modular network consisting of two interacting subnetworks. The nodes within each module are coupled by directed links into a network with a certain topology: (a) a random Erdös-Rényi network, (b) a small-world Watts-Strogatz network, and (c) a scale-free Barabási-Albert network. Intermodule interaction is organized by a relatively small number of random excitatory connections.

case, a link directed from node i to node j is created as well as a link from a randomly chosen node h to node i (for details, see Ref. [30]). In all the cases we use $p_{\rm dir} = 0.5$, however, the results remain qualitatively unchanged for other values of $p_{\rm dir}$ as our calculations show. We briefly describe the algorithms for creating complex networks we used as modules not emphasizing whether the connections are directed or indirected.

1. Random Erdös-Rényi network

The only parameter characterizing the network of N nodes with this topology is the probability $p_{\rm ER}$. We look over all possible pairs of nodes in the network, and with probability $p_{\rm ER}$ a new connection between them appears. The average number of connection per one node (the average degree of nodes) is equal to $k = Np_{\rm ER}$ [34].

2. Small-world Watts-Strogatz network

The parameters characterizing a network of N nodes with a small-world topology is a number of neighboring nodes $k_{\rm edge}$ (taken to be even) in the initial network and the rewiring probability $P_{\rm rew}$. First, a regular ringlike network is created where each node is connected with $k_{\rm edge}$ nearest neighboring nodes ($k_{\rm edge}/2$ from both sides) by bidirectional links. Then we look over all existing links and with probability $P_{\rm rew}$ the connection directed from node i to node j breaks and a new connection is created from node i to another randomly chosen node h [4].

3. Scale-free Barabási-Albert network

A scale-free network of N nodes is created in several stages. First, an initial network of m_0 coupled nodes is created, then the rest of the $N - m_0$ nodes are added to the network one at a time and connected to $m \leqslant m_0$ already existing nodes according to the rule of preferential attachment: m nodes which receive connections from a node newly added are chosen with probability equal to $k_i / \sum k_j$. Here k_i is the degree of the ith node from m existing nodes at the current moment, and the sum $\sum k_j$ is taken over the degrees of all m already existing nodes [35].

In the following we consider modular networks whose modules have the same topology of one of the described types. The connections between the modules are created by the same principle as in random Erdös-Rényi networks. We look over all possible pairs of nodes which belong to different modules and with probability 5% create a link. In addition, we impose a restriction that only excitatory neurons can send directed connections to another module. All the numerical results presented in the paper were obtained for the networks of $2N = 200$ neurons, however, we also considered larger modular networks and they gave qualitatively the same characteristics.

B. Dynamics of nodes

Nodal dynamics in our model are described by the following system of maps [31,32] which allow us to take into account basic properties of individual neuron dynamics:

$$\begin{aligned} x_{n+1} &= x_n + F(x_n) - \beta H(x_n - d) - y_n + I_n^{\rm syn}, \\ y_{n+1} &= y_n + \varepsilon(x_n - J). \end{aligned} \tag{1}$$

Here $n = 0,1,2,\ldots,$ is discrete time, the variable x qualitatively describes the dynamics of the neural membrane potential, and y is responsible for a total action of ionic currents (the recovery variable). The positive parameter ε defines a rate for the recovery variable; the parameters β, d, and J control the shape of a signal generated. Note that the model is based on a discrete version of the FitzHugh-Nagumo system well known in neurodynamics with a cubic nonlinearity $F(x)$ and the additionally introduced Heaviside step function $H(x)$:

$$F(x) = x(x - a)(1 - x), \tag{2}$$

$$H(x) = \begin{cases} 1, & x \geqslant 0, \\ 0, & x < 0. \end{cases} \tag{3}$$

The term $I_i^{\rm syn}$ defines the synaptic current and consists of three parts

$$I_i^{\rm syn} = I_i^{\rm rand} + I_i^{\rm in} + I_i^{\rm out}, \tag{4}$$

where $I_i^{\rm rand}$ takes into consideration small random fluctuations: a sequence $I_{i,n}^{\rm rand}$, $n = 0,1,\ldots,$ is a white Gaussian noise with zero mean and a standard deviation $\sigma_{\rm cur}$. The meaning of the other terms in Eq. (4) will be explained below.

The phase portrait illustrating trajectories corresponding to the regime of spiking oscillations is shown in Fig. 2(a). The system in this case has a unique stable fixed point O [the intersection of the curve $y = F(x)$ and the line $x = J$]. When a relatively small noise $I_i^{\rm rand}$ is applied, phase trajectories move in the vicinity of the fixed point O, and this corresponds to the subthreshold activity of a neuron. With increasing noise intensity the trajectories move to the right in the phase plane, pass the excitation threshold, reach the discontinuity line $x = d$, and return to the vicinity of the stable fixed point. Such a motion in the phase plane corresponds to the generation of an action potential, or spike.

By varying the values of the excitation parameter J and noise intensity $\sigma_{\rm cur}$, one can change the average rate of spiking oscillations in the sequences generated. Figures 2(b) and 2(c) show the waveforms for two values of J and the same noise intensity, and one can see that for higher levels

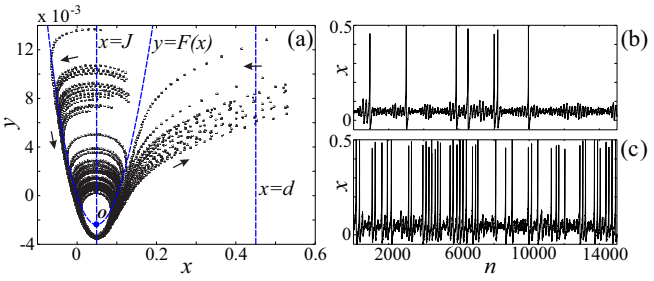

FIG. 2. (Color online) Phase portrait of the map (1) for $a = 0.1$, $\varepsilon = 10^{-4}$, $\beta = 0.5$, $d = 0.4$, $J = 0.04$, and $\sigma_{\rm cur} = 10^{-3}$. Waveforms of the map (1) for different excitation levels (b) $J = 0.04$ and (c) $J = 0.044$.

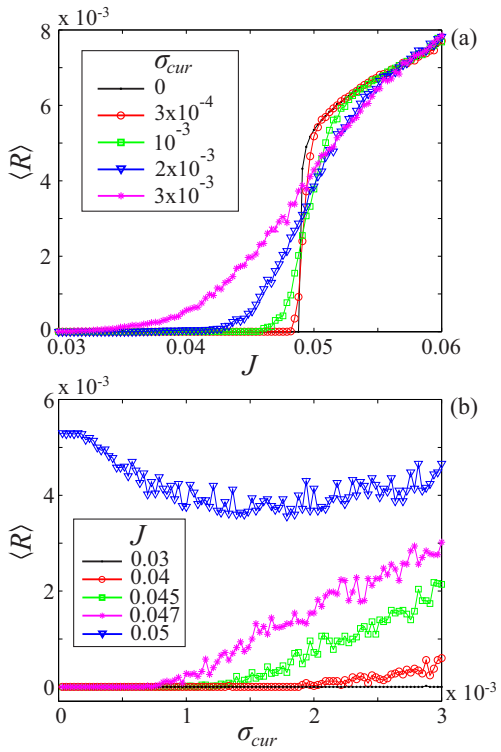

FIG. 3. (Color online) Average spiking rate $\langle R\rangle$ (a) as a function of the excitation parameter J for different noise intensities σ_{cur} and (b) as a function of σ_{cur} for different values of J.

of excitation, spiking oscillations of larger frequency are generated. An analogous effect is observed when increasing the noise intensity σ_{cur}: the average spiking frequency also rises.

Oscillatory properties of the system (1) are summarized in Fig. 3 where the average spiking rate $\langle R\rangle$ as a function of J is plotted for several values of the noise intensity σ_{cur} [Fig. 3(a)] and as a function of σ_{cur} for several values of J [Fig. 3(b)]. Note that in a purely deterministic case ($\sigma_{\text{cur}} = 0$) a sharp transition is observed from the rest state to the spiking activity due to the threshold properties of the model. When small noise is applied the monotonically increasing function $\langle R\rangle(J)$ becomes smoother [Fig. 3(a)]. The effect of noise on the system (1) for different values of J can be different as it follows from Fig. 3(b). We are interested in the case where with increasing σ_{cur} the spiking rate $\langle R\rangle$ rises ($J = 0.04; 0.045; 0.047$) and we use this particular regime of the system (1) when studying the network activity in this paper.

Consider the meaning of the second and the third terms in Eq. (4). The second part of the synaptic current describes the intramodule interaction

$$I_i^{\text{in}} = -g_{\text{in}} \sum_{j=1}^{N} c_{i,j} S[x_j,\theta)(x_i - \nu)], \tag{5}$$

where $c_{i,j}$ is the adjacency matrix with elements equal to 1, if the presynaptic neuron j effects the postsynaptic one i, and equal to 0 in the opposite case. If the presynaptic neuron j sends excitatory (inhibitory) connections then the coupling strength is $g_{\text{in}} = g_{\text{exc}}$ ($g_{\text{in}} = g_{\text{inh}}$) and the reversal potential is $\nu = \nu_{\text{exc}}$ ($\nu = \nu_{\text{inh}}$). Note that each module is characterized by its own adjacency matrix, i.e., there are two (intramodule) matrices in the system, however, we do not introduce any extra notations, for brevity.

The function $S(x,\theta)$ has a sigmoidal form and determines threshold properties of the connections. In the simplest case, we use $S(x,\theta) = H(x-\theta)$ and $\theta = d$. When the presynaptic neuron j displays some activity below the threshold ($x_j < \theta$), the postsynaptic neuron i does not receive input current from that neuron. In the opposite case, when the presynaptic neuron generates signals above the threshold ($x_j > \theta$), i.e., generates action potentials, then the synapse becomes active and affects the postsynaptic neuron i.

The third part of the synaptic current in Eq. (4) describes intermodule interaction

$$I_i^{o} = -g_o \sum_{j=1}^{N} d_{i,j} S(x_j,\theta)(x_i - \nu_{\text{exc}}), \tag{6}$$

where $d_{i,j}$ is an adjacency matrix defined as $c_{i,j}$, except that it describes the influence of a presynaptic neuron j from one module on a postsynaptic neuron i from another one. Note that there are actually two matrices $d_{i,j}$, one describing the influence of the neurons from the first module on those of the second one and another describing the opposite influence. The parameter g_o determines the strength of intermodule coupling, and the reversal potential is always chosen equal to ν_{exc} because the intermodule interaction is performed only by excitatory connections.

To take into account the variety of dynamical regimes observed in real neuron structures, the values of J are chosen randomly and normally distributed in the interval around the value J_0 and the standard deviation $\triangle J = 0.01$. In such a mode, different neurons have different intrinsic oscillatory properties: some of them display only subthreshold activity, others generate irregular spikes with different rates.

Other parameters of the nodal dynamics as well as of the synaptic connections are fixed at the following values: $a = 0.1$, $\beta = 0.5$, $d = 0.45$, $\varepsilon = 0.002$, $\theta = 0.3$, $g_{\text{inh}} = 0.04$, $\nu_{\text{inh}} = -0.2$, $g_{\text{exc}} = 0.01$, and $\nu_{\text{exc}} = 0.6$.

III. NETWORK DYNAMICS

A. Impact of delay

We analyze the influence of network modularity on the collective dynamics so first we are interested in a role of the parameters of intermodule interaction: the coupling strength and delay. The parameters of intramodule coupling and individual dynamics are chosen in such a way that each module separately displays incoherent activity [see the collective dynamics of noninteracting WS modules in Figs. 4(a) and 4(b)], which is achieved by relatively weak intramodule connections and different J values for network nodes ($J_0 = 0.045, \triangle J = 0.01$).

Adding intermodule connections (so far without delay), as it was described above, leads to the fact that the average module activity becomes synchronous rhythmic oscillations when the coupling strength g_o exceeds some critical value [Figs. 4(c) and 4(d)]. In what follows these oscillations are called bursts of average activity, or group bursts, and we

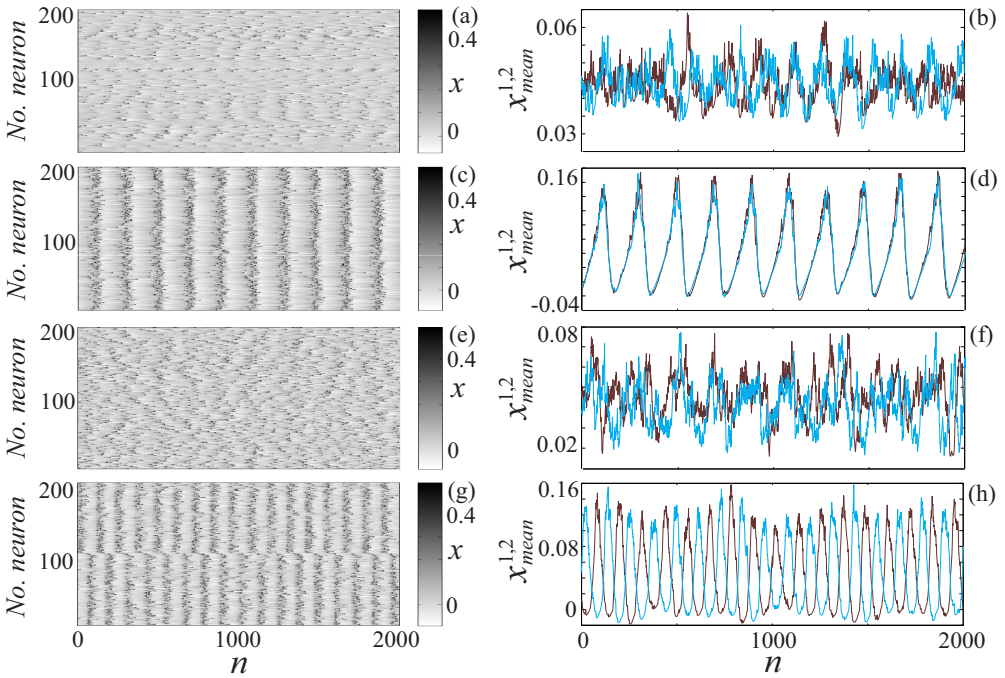

FIG. 4. (Color online) Spike rastrograms (left) and the average module activity (right). (a,b) Two uncoupled modules. (c,d) Coupled modules for $g_o = 0.02$ and in the absence of time delay. (e,f) The same coupling strength, the delay is $\tau = 30$. (g,h) The same coupling strength, the delay is $\tau = 50$.

distinguish in them active phases: time intervals during which the averaged module activity is above $x = J_0$, and passive phases in between the active ones. At the nodal level, spike events mainly happen during the active phases of group bursts, however, the irregularity of the individual dynamics remains and there is no strict periodicity of the individual oscillations.

If a small time delay is introduced into the intermodule coupling then the regime of synchronous group bursts remains almost unchanged. For some critical value of the time delay, the neuronal dynamics becomes incoherent [see Figs. 4(e) and 4(f)] as it was in the case of uncoupled modules, but in long enough time series one can find short intervals during which synchronous group bursts appear. A further increase in the time delay leads to a regime of rhythmic oscillations [Figs. 4(g) and 4(h)], however, in the form of antiphase group bursts whose average frequency is markedly higher than that of the inphase bursts at small delays [Figs. 4(c) and 4(d)]. Thus, with increasing time delay in the intermodule coupling, the inphase group activity is replaced by the antiphase one as well as one observes the change in the frequency of group oscillations.

To characterize the module synchronization degree, we use a relatively simple method proposed by the authors of Refs. [36,37] for quantifying synchronization of bursting oscillations. For a long time series of the network dynamics, we calculate time intervals T_1^j (see Fig. 5) during which the average activity of the first module $X^{(1)} = 1/N \sum_{i=1}^{N} x^{(i,1)}$ is above some threshold value x_{th} (we set it equal to J_0). The total sum of these intervals gives T_1. Analogously, for the second group, intervals T_2^j are computed and they give T_2. Then we measure time intervals T_{12}^k during which both the group activities are simultaneously above the threshold: $\{X^{(1)} > x_{\rm th}\} \cap \{X^{(2)} > x_{\rm th}\}$. Summing them up we obtain T_{12}, the total time of group burst overlapping. The quantity σ defined as

$$\sigma = \frac{1}{2}\left(\frac{T_{12}}{T_1} + \frac{T_{12}}{T_2}\right), \tag{7}$$

gives an averaged fraction of overlapping bursts in the total time of superthreshold activity of one module. The values of σ close to unity correspond to the inphase intermodule synchronization, and those close to zero indicate the antiphase intermodule synchronization.

We have analyzed the spectra of group activity and the regimes of modular synchronization depending on the time delay for the three intramodule topologies considered, the results are shown in Fig. 6. Despite the difference in the intramodule connectivity, the impact of the delayed coupling is qualitatively similar for all three cases. One can distinguish in Fig. 6 the delay intervals labeled by the Roman numerals corresponding to different types of collective dynamics. In the intervals I and V where the values of σ are close to 1, there is the

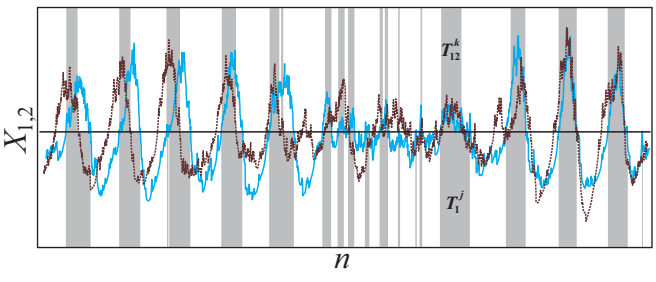

FIG. 5. (Color online) Definition of the synchronization degree σ.

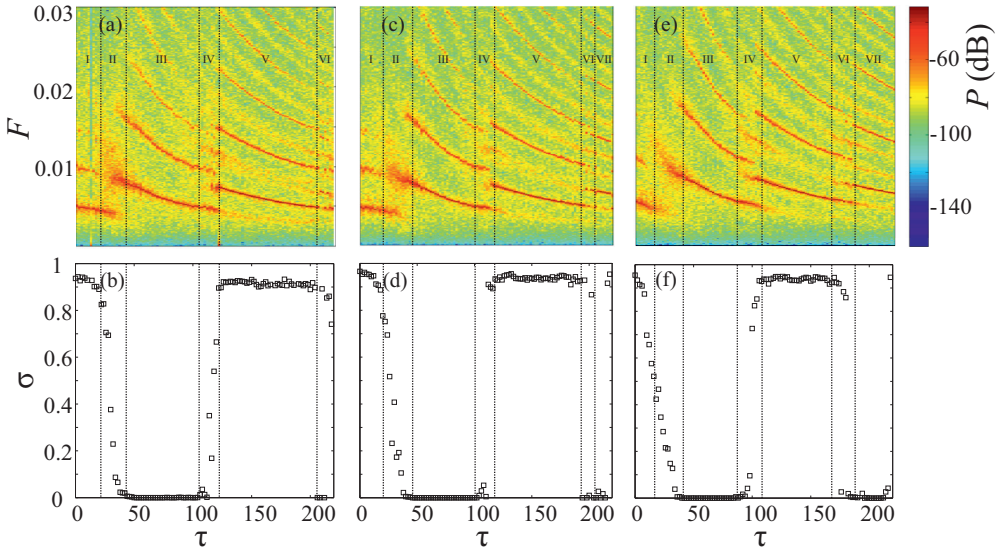

FIG. 6. (Color online) (a), (c), and (e) Spectrogram of the average module activity depending on the intermodule coupling delay τ. (b,d,f) Module synchronization degree $\sigma(\tau)$ for $J_0 = 0.045$ and $g_o = 0.02$. The intramodule connection topology is (a,b) random Erdös-Rényi ($p_{\mathrm{ER}} = 0.2$), (c,d) small-world Watts-Strogatz ($k_{\mathrm{edge}} = 10$, $P_{\mathrm{rew}} = 0.1$), and (e,f) scale-free Barabási-Albert ($m_0 = m = 2$).

inphase regime of modular synchronization. In the intervals III and VI where σ is close to zero, there is the antiphase regime. The intervals II, IV, and VI correspond to transient regimes where the modules display incoherent activity without any pronounced rhythm. Note that in the intervals of the inphase and antiphase regimes, the frequency of lower harmonic as well as its multiples decreases with increasing delay. At the transition from one regime (e.g., antiphase in the interval III) to another (inphase in the interval V), the frequency abruptly rises, and the magnitude of the jump is higher for smaller time delays. It is interesting to note that the width of the interval I corresponding to the inphase group bursts at a small delay, is always less than that of other intervals, in particular, the interval V where there is also the inphase regime.

B. Impact of other parameters

Consider how the collective dynamics described depends on the intermodule coupling strength g_o and the average nodal excitation level J_0. For brevity, we discuss further the modular network consisting of small-world Watts-Strogatz subnetworks. The other two types of intramodule topology give qualitatively similar results; thus what is said below equally refers to all three intramodule topologies considered in this paper.

For three typical regimes (inphase, antiphase, and transient) we plotted spectrograms for different time delays and calculated the synchronization degree σ depending on g_o and J_0. In delay intervals corresponding to the inphase regime at small g_o not exceeding some threshold value there are no pronounced rhythmic module oscillations so one cannot speak of group burst synchronization in this case. For $\tau = 10$ in Fig. 7(a) this threshold is approximately equal to $g_o = 0.01$. The same result follows from the function $\sigma(g_o)$ at $g_o < 0.01$: the values of σ do not exceed 0.8 [Fig. 8(a), $\tau = 10$)]. By increasing the intermodule coupling strength g_o, one observes a decrease in the average frequency of the collective oscillations [Fig. 7(a)], and the value of σ approaches unity [Fig. 8(a)]. It should be noted that the burst frequency decreasing with the coupling strength is characteristic only for the first interval of time delay corresponding to the inphase regime. As we show below, in the inphase regimes for greater time delays the frequency of group bursts rises with increasing g_o.

The parameter J_0 affects the collective behavior as follows. Below some threshold value J_0, spike events in the network are relatively rare, and these individual oscillations are not enough for the average group bursts to be generated. For the case shown in Figs. 7(b) and 8(b) ($\tau = 10$), this threshold value is about $J_0 = 0.04$, so below it one does not observe pronounced harmonics in the spectrum [Fig. 7(b)] and the values of σ are less than 1 [Fig. 8(b) ($\tau = 10$)].

In the intervals of time delay corresponding to the antiphase regime, the emergence and synchronization of group bursts depend on the coupling strength g_o also in a threshold fashion. In Figs. 7(e) and 8(a) ($\tau = 50$) this threshold value is equal approximately $g_o = 0.01$ for the intermodule coupling delay $\tau = 50$. The value of σ decreases to zero which means that the group bursts are antiphase [Fig. 8(a) ($\tau = 50$)], and their average frequency gradually rises with increasing coupling strength g_o [Fig. 7(e)].

The transient regime is characterized by diffuse spectrograms [Figs. 7(c) and 7(d)] and by values of σ greater than zero but smaller than 1 [Figs. 8(a) and 8(b) ($\tau = 30$)], which indicates the absence of coherent module activity. However, for large enough values of g_o and J_0, the spectrograms in Figs. 7(c) and 7(d) are mixes of the spectrograms shown in Figs. 7(a) and 7(b) and 7(e) and 7(f). For example, in Fig. 7(c) one can distinguish a low-frequency harmonic decreasing with g_o and another (high-frequency) one increasing with g_o. These intervals of g_o and J_0 correspond to a bistable regime where in a long enough time series one can find almost synchronous low-frequency group bursts, high-frequency antiphase bursts, and periods of incoherent activity.

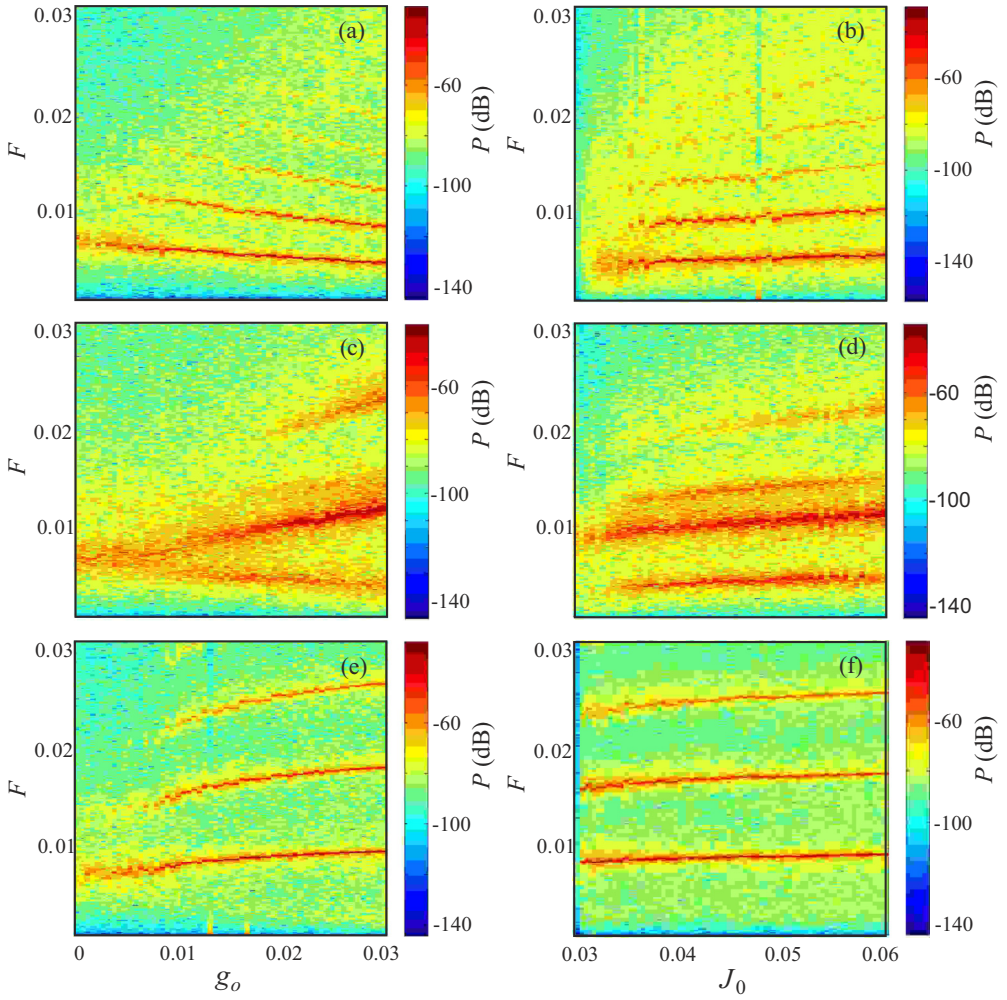

FIG. 7. (Color online) Spectrograms of the average module activity depending on (a,c,e) the intermodule coupling strength g_o (for $J_0 = 0.045$) and (b,d,f) the average excitation level J_0 (for $g_o = 0.02$) in different regimes of the group activity: (a,b) inphase ($\tau = 10$), (c,d) transient ($\tau = 30$), and (e,f) antiphase ($\tau = 50$).

The impact of the intermodule coupling delay and strength on a synchronization regime and the frequency of bursts generated is summarized in Fig. 9. The two-parameter diagrams show the alternation of the inphase and antiphase regimes [Fig. 9(a)], as well as the decrease in the frequency of the first harmonic F_b of group bursts within each of these regimes with increasing τ [Fig. 9(b)]. Note that an unobvious result follows from Fig. 9(b): with increasing intermodule coupling strength g_o, the frequency of group bursts increases for a fixed delay,

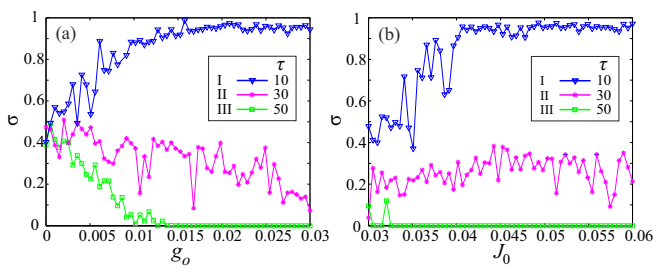

FIG. 8. (Color online) Synchronization degree σ versus (a) g_o and (b) J_0 for different time delays τ of intermodule coupling.

while in the first zone of inphase regime the opposite case takes place, a decrease in the frequency with increasing g_o.

To understand how the indicated features of collective network dynamics are connected to individual nodal oscillations, we consider the average spiking rate for different parameters. We define the average spiking rate $\langle R \rangle$ as a total number of spikes generated by all the network nodes during a long enough time interval T over this interval T and a total number $2N$ of nodes in the network. Figure 10 shows $\langle R \rangle$ as a function of the coupling strength and the excitation level for delays corresponding to three different regimes of modular synchronization. Note that in all the cases the spiking rate rises on the average with increasing g_o as well as J_0. The rate $\langle R \rangle$ in the antiphase regime ($\tau = 50$) exceeds almost twice $\langle R \rangle$ in the inphase regime ($\tau = 10$) starting from some coupling strength g_o [Fig. 10(a)]. To some extent, this result correlates with the spectra of group bursts where the frequency of collective oscillations rises with increasing g_o [Figs. 8(a) and 9(b)], however, for the first interval of time delays the functions $F_b(g_o)$ and $\langle R \rangle(g_o)$ behave differently. While the frequency of group bursts is a decreasing function of the intermodule coupling strength, the spiking rate is an increasing

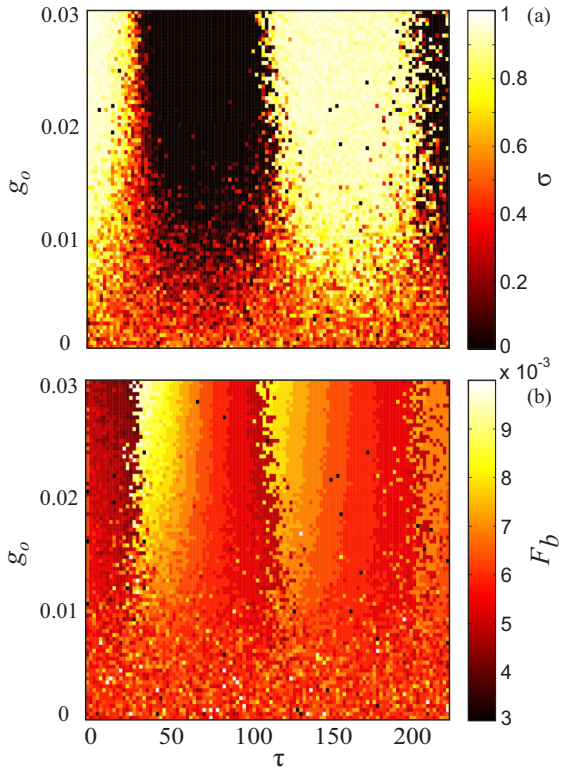

FIG. 9. (Color online) (a) Dependence of the synchronization degree σ and (b) the frequency of the first harmonic of group bursts F_b on τ and g_o.

function of g_o [cf. Figs. 7(a) and 10(a)]. Thus one concludes that the observed collective phenomena cannot be reduced to the dynamical properties of individual nodes but emerge as a result of their interaction.

Now consider in what range changes the amplitude of collective oscillations depending on g_o and J_0 in different regimes of modular synchronization. By an amplitude we understand here the difference between the maximum and minimum values of the mean field for one module [Var(X_1)] or the whole network [Var(X_{12})]. Note that all the characteristics shown in Fig. 11 are on the average increasing functions of g_o and J_0, so with increasing these parameters not only the spiking rate increases [Fig. 10(a)] but also the amplitude. From Figs. 11(a) and 11(c) with functions Var(X_1) and Var(X_{12}) it follows that averaging the activity in the inphase regime (I) over one module as well as over the whole network leads to

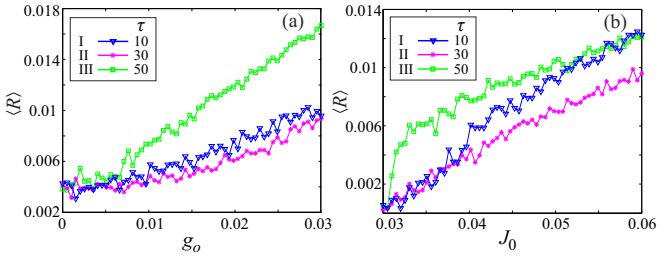

FIG. 10. (Color online) Average spiking rate $\langle R\rangle$ depending on (a) g_o and (b) J_0 for different time delays τ.

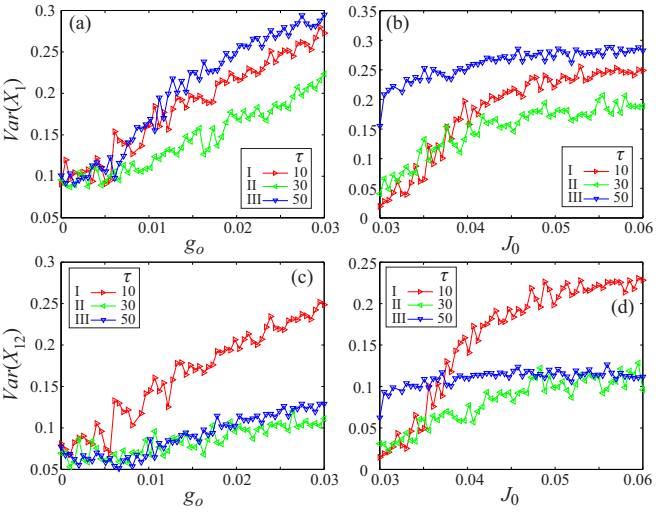

FIG. 11. (Color online) Amplitude of the average module activity Var(X_1) versus (a) g_o and (b) J_0, and the amplitude of the average whole-network activity Var(X_{12}) versus (c) g_o and (d) J_0 for different time delays τ.

the same result which means the coherent behavior of the two modules. In contrast, in the antiphase and transient regimes the values of Var(X_{12}) are almost two times lower than Var(X_1), i.e., one module compensates another. Analogous conclusions can be made from the comparison between Figs. 11(b) and 11(d).

The observations presented above allow us understand possible dynamic mechanisms underlying the impact of the delayed coupling in the collective activity of modular neural networks. For small time delays starting from some critical coupling strength, the neurons of both modules generate spikes mostly during the same time periods, thus producing inphase bursts of the average modular activity. Increasing the coupling delay results in that the information about the activation of one module comes later to another module and vice versa, therefore the group bursts become wider and the frequency of modular inphase oscillations becomes smaller. With a further increase of delay, the time needed for information propagation from one module to another becomes insufficient for simultaneous activation of the both modules and a new regime appears: antiphase group burst oscillations with a period about twice greater than the current coupling delay. The coupling with larger delays produces antiphase module oscillations with a larger period which is still about two times greater than the delay. After that the inphase regime appears with a period equal approximately to the coupling delay, and with a further increase of delay the frequency decreases due to the described mechanism. The same mechanisms take place at larger coupling delays for transitions between different synchronization regimes and for the frequency decrease within delay intervals corresponding to particular regimes.

IV. CONCLUSION

In this paper, we considered modular networks of interacting neuron-like elements which generate irregular spike sequences. The connections between the elements within one

module reproduce directed excitatory or inhibitory influence through chemical synapses. The connection topology of intramodule coupling is chosen from one of the three types: random Erdös-Rényi, small-world Watts-Strogatz, or scale-free Barabási-Albert network; the intermodule connections are organized in the form of relatively sparse directed excitatory links. We found a dual role of the intermodule coupling delay in the collective network dynamics. First, with increasing time delay, inphase and antiphase regimes, where individual spikes form rhythmic modular burst-like oscillations, alternate with each other. Second, the average frequency of the collective oscillations in each of these regimes decreases with increasing intermodule coupling delay. An increase in the intermodule coupling strength and the network excitation level leads to an enhancement of synchronization in the inphase as well as antiphase regimes. The frequency of group bursts rises with increasing intermodule coupling strength for all delay intervals except the first one: for a small time delay in the inphase regime the frequency decreases with increasing coupling strength.

ACKNOWLEDGMENT

This work was supported by the Russian Science Foundation (Project No. 14-12-01358).

[1] A. Schnitzler and J. Gross, Nat. Rev. Neurosci. **6**, 285 (2005).
[2] P. J. Uhlhaas and W. Singer, Neuron **52**, 155 (2006).
[3] M. Girvan and M. E. J. Newman, Proc. Natl. Acad. Sci. USA **99**, 7821 (2002).
[4] D. J. Watts and S. H. Strogatz, Nature (London) **393**, 440 (1998).
[5] A. Arenas, A. Diaz-Guilera, J. Kurths, Y. Moreno, and C. Zhou, Phys. Rep. **469**, 93 (2008).
[6] E. Bullmore and O. Sporns, Nat. Rev. Neurosci. **10**, 186 (2009).
[7] V. V. Klinshov and V. I. Nekorkin, Phys. Usp. **56**, 1217 (2013).
[8] E. Schöll, in *Advances in Analysis and Control of Time-Delayed Dynamical Systems*, edited by J. Q. Sun and Q. Ding (World Scientific, Singapore, 2013), pp. 57–84.
[9] Q. Y. Wang, M. Perc, Z. S. Duan, and G. R. Chen, Phys. Rev. E **80**, 026206 (2009).
[10] N. F. Rulkov, Phys. Rev. Lett. **86**, 183 (2001).
[11] Q. Y. Wang and G. R. Chen, Chaos **21**, 013123 (2011).
[12] Q. Wang, G. Chen, and M. Perc, PLoS ONE **6**, e15851 (2011).
[13] T. Perez, G. C. Garcia, V. M. Eguiluz, R. Vicente, G. Pipa, and C. Mirasso, PLoS ONE **6**, e19900 (2011).
[14] H. Yu, J. Wang, C. Liu, B. Deng, and X. Wei, Physica A (Amsterdam, Neth.) **392**, 5473 (2013).
[15] H. Yu, J. Wang, Q. Liu, J. Sun, and H. Yu, Chaos, Solitions & Fractals **48**, 68 (2013).
[16] Y. Qian, Y. Zhao, F. Liu, X. Huang, Z. Zhang, and Y. Mi, Commun. Nonlinear Sci. Numer. Simulat. **18**, 3509 (2013).
[17] C. Liu, J. Wang, L. Wang, H. Yu, B. Deng, X. Wei, K. Tsang, and W. Chan, Chaos, Solitions & Fractals **59**, 1 (2014).
[18] A. Nordenfelt, J. Used, and M. A. F. Sanjuán, Phys. Rev. E **87**, 052903 (2013).
[19] L. Zemanová, C. Zhou, and J. Kurths, Physica D **224**, 202 (2006).
[20] C. A. S. Batista, E. L. Lameu, A. M. Batista, S. R. Lopes, T. Pereira, G. Zamora-López, J. Kurths, and R. L. Viana, Phys. Rev. E **86**, 016211 (2012).
[21] E. L. Lameu, C. A. S. Batista, A. M. Batista, K. Iarosz, R. L. Viana, S. R. Lopes, and J. Kurths, Chaos **22**, 043149 (2012).
[22] C. Liu, J. Wang, H. Yu, B. Deng, X. Wei, K. Tsang, and W. Chan, Chaos **23**, 033121 (2013).
[23] C. Liu, J. Wang, H. Yu, B. Deng, X. Wei, J. Sun, and Y. Chen, Chaos, Solitons & Fractals **47**, 54 (2013).
[24] I. Kanter, E. Kopelowitz, R. Vardi, M. Zigzag, W. Kinzel, M. Abeles, and D. Cohen, Europhys. Lett. **93**, 66001 (2011).
[25] R. Vardi, R. Timor, S. Marom, M. Abeles, and I. Kanter, Europhys. Lett. **93**, 60003 (2011).
[26] E. Kopelowitz, M. Abeles, D. Cohen, and I. Kanter, Phys. Rev. E **85**, 051902 (2012).
[27] R. Vardi, R. Timor, S. Marom, M. Abeles, and I. Kanter, Europhys. Lett. **100**, 48003 (2012).
[28] R. Vardi, R. Timor, S. Marom, M. Abeles, and I. Kanter, Phys. Rev. E **87**, 012724 (2013).
[29] R. Vardi, A. Goldental, S. Guberman, A. Kalmanovich, H. Marmari, and I. Kanter, Front. Neural Circuits **7**, 176 (2013).
[30] B. J. Prettejohn, M. J. Berryman, and M. D. McDonnell, Front. Comput. Neurosci. **5**, 11 (2011).
[31] V. I. Nekorkin and L. V. Vdovin, Izv. Vyssh. Uchebn. Zaved. Prikladn. Nelinejn. Din. **15**, 36 (2007).
[32] M. Courbage, V. I. Nekorkin, and L. V. Vdovin, Chaos **17**, 043109 (2007).
[33] M. L. Feldman, *Cellular Components of the Cerebral Cortex* (Plenum, New York, 1984).
[34] P. Erdös and A. Rényi, Publ. Math, Inst. Hung. Acad. Sci. **5**, 17 (1960).
[35] A.-L. Barabási and R. Albert, Science **286**, 509 (1999).
[36] V. I. Nekorkin and O. V. Maslennikov, Radiophys. Quantum Electron. (Engl. Transl.) **54**, 56 (2011).
[37] M. Courbage, O. V. Maslennikov, and V. I. Nekorkin, Chaos, Solitons & Fractals **45**, 645 (2012).